Divergent CD8 memory T cell subsets in an encephalitis model of *Toxoplasma gondii* infection

Magali M. Moretto, Keer Chen, Christina Cox, Jie Chen, Imtiaz A Khan.

Department of Microbiology, Immunology, and Tropical Medicine, The George Washington University, Washington DC, 20037.

*Magali M. Moretto and Imtiaz A Khan.

Email: morettom@gwu.edu, imti56@gwu.edu.

Author Contributions: M.M. and I.K. designed the research, M.M., K.C., and J.C. performed the experiments, M.M., K.C., and C.C. analyzed the data, and M.M. and I.K. wrote the manuscript.

Competing Interest Statement: The authors declare no competing interests.

Classification: Biological Sciences, Immunology and Inflammation.

Keywords: Toxoplasma gondii, CD8 T cells, memory T cells, stem-like T cells, exhaustion.

This PDF file includes:

Main Text

Figures 1 to 5

Abstract

Toxoplasma gondii is a foodborne pathogen with important human implications. Polyfunctional CD8 T cell immunity is critical for keeping the chronic infection under control. However, in susceptible animals, T-cell exhaustion leads to the reactivation of the infection. Phenotypic and transcriptomic analyses of the polyclonal antigen-specific CD8 T cell response in these mice define four different subsets based on KLRG1 and CD62L expression. While pop1 ($KLRG1^{+}CD62L^{lo}$) bears the characteristics of a terminal effector population, pop3 ($KLRG1^{-}CD62L^{hi}$) resembles stem-like CD8 T cells described in other models and can transition into pop1 either directly or via pop2 ($KLRG1^{-}CD62L^{lo}$) and pop4 ($KLRG1^{+}CD62L^{hi}$). Interestingly, despite sharing several surface markers and being derived from pop3, intermediate effector/memory pop4 exhibits strong genetic similarities with pop1 with only a 43 differentially expressed genes divergence between the two populations. Although all memory subsets (pop2-4) display elevated inhibitory receptors, pop4 also exhibits increased levels of costimulatory molecules. Therefore, this subset maintains its functional fitness even during the late chronic infection when other subsets including pop1 become dysfunctional. Overall, our

studies demonstrate that stem-like memory CD8 T cells (pop3) develop early after infection when the pop1 effector subset is still functional. Significantly, pop3 gives rise to an exhausted dysfunctional pop2 but more importantly, is a source of highly functional pop4. However, despite the generation of a complex CD8 T cell response, the susceptible host is ultimately unable to contain *T. gondii* and prevent encephalitis.

Significance Statement

Toxoplasma gondii infection causes encephalitis in susceptible and immunocompromised hosts. Polyfunctional CD8 T cells are critical for long-term control of the infection and can be segregated into four different subsets based on KLRG1 and CD62L expression. The heterogenous CD8 T cell population consists of terminally differentiated effector, intermediate effector/memory, exhausted/dysfunctional memory, and stem-like memory subsets. Most of these subsets display plasticity, especially the stem-like memory CD8 T cells that convert into all other populations. Our study provides important insights into the complexity of the memory CD8 T cell response during chronic toxoplasmosis and identifies the CD8 T cell subsets that need to be targeted to keep the infection under control.

Main Text

Introduction

CD8 T cell immunity plays a critical role in the protection against intracellular pathogens and malignancies (1, 2). Upon TCR engagement and co-stimulation by antigen-presenting cells, naïve CD8 T cells differentiate into effector and memory effector precursor effector (MPEC) CD8 T cells (3). Terminally differentiated effector CD8 T cells provide immediate protection and contract once pathogens or tumors are controlled (4). On the other hand, memory CD8 T cells derived from MPEC are long-lived and provide long-term protection against recuring infections (5). Previously, memory CD8 T cells were categorized into T_{CM} (central memory) and T_{EM} (effector memory) populations based on CCR7 and CD62L expression (6). T_{CM} ($CD62L^{hi}CCR7^{hi}$) exhibits increased longevity, greater homeostatic proliferation, and recall response (7). In comparison, T_{EM} ($CD62L^{lo}CCR7^{lo}$) has a shorter life span and displays increased cytokine production and cytotoxic activity (7). This paradigm became more complex as additional populations like tissue-resident memory, stem-like memory, and hybrid memory CD8 T cells have also been identified (8, 9). Stem-like CD8 T cells are long-lived with self-renewal capability and demonstrate a high level of plasticity. In the context of chronic infections or cancer, constant antigenic stimulation impairs the memory CD8 response as a result, cells become exhausted and subsequently undergo apoptosis (10). Interestingly, in these

conditions, stem-like CD8 T cells, due to their plasticity can replenish the CD8 T cell response and are therefore critical for controlling chronic infection and cancer (11).

Toxoplasmosis, caused by the obligate intracellular parasite *T. gondii*, is a chronic infection that affects up to a third of the world's population (12). Long-term protection is predominantly dependent on the CD8 T cell memory population, and their functionality, like cytotoxic activity and IFNγ production, is critical for keeping the chronic infection under control (13). While BALB/c mice (H-2L^{d}) are resistant to toxoplasmosis, C57BL6 (H-2K^{b}), which are susceptible, cannot control the chronic infection and develop encephalitis (14). Interestingly, in a resistant model of *T. gondii* infection, effector CD8 T cells are critical for controlling the acute infection and are continuously generated even after chronicity is achieved (15). The persistent effector response is maintained by an intermediate population with a memory-effector hybrid phenotype that is dependent on antigen persistence. Uninterrupted effector response may be necessary as, contrary to earlier beliefs, parasites continue to replicate even after the chronic infection is established (16). The situation is probably more complex in an encephalitis model where CD8 T cell exhaustion has been reported and the host cannot control the chronic infection (13).

Using a susceptible C57BL6 model, the present study demonstrates that the memory CD8 T cell response cannot be categorized based on CD62L and CCR7 expression. However, using a clustering algorithm, CD8 T cells can be divided into four subsets with differential KLRG1 and CD62L expression: KLRG1^{+}CD62L^{lo} (pop1), KLRG1^{-}CD62L^{lo} (pop2), KLRG1^{-}CD62L^{hi} (pop3), and KLRG1^{+}CD62L^{hi} (pop4). Pop1 resembles a classic effector subset, pop2 is similar to T_{EM}, pop3 is a stem-like memory subset, and pop4 is an intermediate effector/memory population. Adoptive transfer studies demonstrate the plasticity of stem-like pop3, which can generate effector pop1 directly or via pop4 and pop2. Interestingly, effector/memory pop4 is more functional than effector pop1 as early as week 2 post-infection (p.i.), and its fitness is sustained during the chronic phase of the infection. These results demonstrate the heterogeneity of the memory CD8 T response in a susceptible encephalitis model when the host is unable to restrict the chronic infection.

Results

CD62L and KLRG1 expression defines four antigen-experienced CD8 T cell subsets in *T. gondii* infected animals

Antigen-experienced (Ag^{+}) memory CD8 subsets were analyzed using a published surrogate marker strategy (CD44^{hi}CD11a^{hi})(17, 18), since there is currently only one tetramer (tet^{+}: Tgd057) that recognizes a small fraction of Ag^{+} cells in the spleen of chronically infected

C57BL6/J mice (19) (Fig. S1A). The surrogate marker approach identifies 10% or less CD8 T cells from naïve mice and facilitates the identification of polyclonal CD8 T cell response in *T. gondii* infected animals while identifying only 10% or less CD8 T cells from naïve mice (Fig. 1D). Furthermore, parallel analysis of Ag^+ and tet^+ ($Tgd057^+$) CD8 T cells at 6 weeks post-infection (p.i.) demonstrates that the majority of tet^+ cells in the brain, liver, and spleen are predominantly $CD44^{hi}CD11a^{hi}$ (Ag^+)(Fig. S1A). These findings confirm previous observations reporting that tet^+ CD8 T cells coexpress CD11a and CD44 and comprise a higher percentage of $IFN\gamma^+$ cells than $CD11^{lo}CD44^{lo}$ CD8 T cells (18). Our data also substantiates the result from a previous study that *T. gondii* infection does not generate classical T_{EM} ($CD62L^{lo}CCR7^{lo}$) and T_{CM} ($CD62L^{hi}CCR7^{hi}$) memory subsets observed in other models (6). Furthermore, as shown in Fig. S1B-C, a significant percentage of memory ($CD127^{hi}$) Ag^+ CD8 T cells from the brain, liver, and spleen of infected mice labeled with CCR7 and CD62L fall outside the established T_{CM}/T_{EM} model. Even though KLRG1, a marker commonly associated with effector CD8 T cells (20), can be expressed by some memory subsets (21, 22), an unexpectedly high frequency of $CD62L^{lo}CCR7^{lo}$ and $CD62L^{hi}CCR7^{hi}$ CD8 T cells express this marker (Fig. S1D). Therefore, unbiased clustering with FlowSOM algorithm was applied to categorize Ag^+ CD8 T cells based on four well-described CD8 T cell subset markers: CD62L, KLRG1, CD127, and CCR7. As shown in Figure 1A, the Ag^+ CD8 T cells were clustered into four populations. Unlike CCR7 and CD127, CD62L and KLRG1 exhibit clear differential expression patterns among the four populations (Fig. 1B-C). Using these two markers, Ag^+ CD8 T cells were segregated into four populations: $KLRG1^+CD62L^{lo}$ (pop1), $KLRG1^-CD62L^{lo}$ (pop2), $KLRG1^-CD62L^{hi}$ (pop3), and $KLRG1^+CD62L^{hi}$ (pop4) (Fig. 1D). Interestingly, these subsets have been previously described in the peritoneal exudate, spleen and brain from mice infected with a vaccine strain of *T. gondii* (19). This report evaluated the role of IL-12 in the regulation of memory CD8 T cells, but the subsets were not further characterized. Next, flow cytometric expression for markers associated with memory and effector responses (CD127, CCR7, CD62L, KLRG1, CX3CR1) by Ag^+ CD8 T cells at week 5 p.i. was visualized using the dimensionality reduction algorithm TriMap (Fig. 1E). When overlayed on the TriMap plot, pop1-4 effectively comprise most of the Ag^+ CD8 T cell population with minimal overlap (Fig. 1F). At week 5 p.i., $KLRG1^+$ pop1 represents the largest subset (in percentage and frequency) while the other three subsets are equally represented (Fig. 1G). As expected, pop1 ($KLRG1^+CD62L^{lo}$) peaks at week 2 p.i., during the acute infection when the parasite is actively replicating and decreases slowly during the chronic phase. However, this subset remains the largest population detected at weeks 5 and 8 p.i. (Fig. 1H). The persistent dominance of pop1 can be caused by the continuous replication of the parasite even during the chronic phase of the infection (16). Similarly, the number of cells in pop2 ($KLRG1^-CD62L^{lo}$) decreases over the course of the infection (Fig. 1H).

Conversely, the numbers of pop3 (KLRG1^{-}CD62L^{hi}) and pop4 (KLRG1^{+}CD62L^{hi}) increase as the infection progresses to chronicity. The different populations were then evaluated in the brain and liver (Fig S2). Pop1 is more predominant at week 2 p.i. when the replicating parasites are disseminating to the different tissues as well as during the late chronic phase of the infection. Nevertheless, pop3 and pop4 are also detected in both organs. The different populations in the spleen were further characterized with various memory/activation markers: CD127, CCR7, CD27, a marker that promotes long-term survival of CD8 T cells (23), activation associated isoform of CD43 (6), CX3CR1, a chemokine receptor associated with cytotoxic effector function in memory CD8 T cell subsets (24), CXCR3, known to regulate stem-like memory and proliferative CD8 T cells, (25), and CXCR5, defined as an effector memory marker in LCMV infection (Fig. 1I-K) (26). As summarized in Figure 1K, pop1 resembles effector T cells with low expression of CD127, while pop2 displays high levels of CD127 and CXCR3 (Fig.1I-J). CD127^{+}Pop3 and pop4, which can be classified as memory subsets, also exhibit CCR7, CXCR5, and CD43. Furthermore, KLRG1^{+} pop1 and pop4 co-express the cytotoxic effector function marker CX3CR1 (Fig 1J). Our data reveals that, in an encephalitis model of natural toxoplasma infection, four distinct subsets are generated, each expressing different activation and chemokine receptors (Fig. 1I-K).

Next, the transcriptional profile of each population was characterized by bulk RNA sequencing during the late chronic phase of the infection when the CD8 T cell response is compromised (27) (week 8 p.i.). The principal component analysis demonstrates that each population displays a unique gene expression signature that differs from the CD8 T cells isolated from naive mice (Fig. 2A). The PCA also reveals that pop1 and pop4 are more alike despite pop4 exhibiting a strong phenotypic resemblance to pop3 (Fig. 1K). A lower Spearman's coefficient factor is observed when comparing pop3 to pop1 or pop4, emphasizing the differences between pop3 and these populations (Fig. 2B). Conversely, higher factors are detected within duplicates as well as between pop1 and pop4 underscoring the PCA results. The Venn diagram also confirms that pop4 has more differentially expressed genes (DEGs) in common with pop1 than pop3 (Fig. 2C). Next, the top 3800 DEGs from the four populations were divided into six clusters using K-means clustering (Fig. 2C-E, Table S1). As pop1 and pop4 share a large part of their transcriptome, only 43 DEGs are dysregulated when comparing the two populations (Fig. 2D), and the expression of Sell, which encodes CD62L, is the most significantly different (adjusted p value= 1.07×10^{-81})(Fig. 2E). DEGs that are exclusively upregulated in pop2 belong to the cluster 1 which contains markers associated with exhaustion like Lag-3, Pdcd1, and Cd160 (Fig. 2F). Genes associated with stem-like cells (Tcf7, Cd69, Cxcr5, and Nt5e) (cluster II) are upregulated in pop3, while those linked to effector T cell differentiation (cluster III) are downregulated in this population. Similar to cluster I, cluster IV is comprised of genes

associated with T cell activation (Cd200, Myc, Icos, and Cd27) with higher expression in pop2 and 3. Genes related to the effector phenotype (perforin, granzymes, T-bet, annexin) are predominantly expressed in pop1 and 4 (cluster V) confirming that pop1 and pop4 have a similar gene expression pattern with a terminal differentiation signature commonly associated with an effector response. Genes from clusters I-V were then analyzed with Metascape to determine the overrepresented biological pathways. Clusters I, II, IV, and V shared several common immune processes (regulation of lymphocyte activation, regulation of cell-cell adhesion, and regulation of lymphocyte proliferation). Similarly, genes associated with the negative regulation of immune response processes were significantly upregulated in clusters I, II, and IV. Interestingly, genes related to translation, especially those encoding ribosomal protein which were recently reported to be associated with stem-like CD8 T cells were enriched in cluster II (28).

Overall, based on phenotypic and transcriptomic analyses, CD8 T cell response during *T. gondii* infection can be segregated into four different subsets. Pop1 displays the hallmark signature of terminally differentiated effector CD8 T cells, and the other three populations display higher CD127 expression associated with memory subsets. Although these memory subsets do not conform to the classical T_{CM}/T_{EM} model, pop2 closely resembles T_{EM} ($CCR7^{lo}CD62L^{lo}$), and pop3 is similar to T_{CM} ($CCR7^{hi}CD62L^{hi}$).

Pop3 bears the characteristics of stem-like memory CD8 T cells and gives rise to multiple CD8 T subset

Next, to determine the plasticity of the different subsets, adoptive transfer studies were performed. The four populations were isolated from CD45.1 mice at week 5 p.i. and individually transferred to equally infected (5 weeks p.i.) congenic (CD45.2) mice. The recipients were sacrificed 6 days post-transfer and the donor population (CD45.1) was characterized (Fig. 3A). As shown in Figure 3 B, a significantly higher number of CD45.1 CD8 T cells is recovered from the mice that received pop3 as compared to the other subsets. The majority of CD45.1 cells recovered from mice transferred with pop1 or pop3 retained their original phenotype (Fig. 3C). However, CD45.1 cells from pop2 recipients partially converted into pop1. Interestingly, the majority of CD45.1 CD8 T cells from pop4 recipients switched to effector pop1 (Fig. 3C).

Subsequently, the plasticity of CD8 T cell subsets in response to recall antigens was assessed by adoptively transferring the populations to naïve animals. The following day the recipients were challenged with *T. gondii* cysts and analysis of the donor population was performed 14

days later (Fig. 3D). Similar to the previous experiment, CD45.1 cells from recipients transferred with pop1 retained their original phenotypes while an increased percentage of CD45.1 CD8 T cells from mice that received pop2 converted into pop1 (Fig. 3F). Akin to the transfer in equally infected mice (Fig. 3E), donor pop4 fully transitioned into pop1. Expectedly, CD45.1 cells recovered from mice transferred with pop3 (stem-like population) converted into every other phenotype. The ability of Pop3 to retain its original characteristics when transferred into a congenic infected recipient as well as convert into pop1, 2, and 4 after challenge, further indicates their resemblance to stem-like CD8 T cells described in viral infection and cancer (29). Therefore, to compare pop3 with previously described stem-like CD8 T cells, RNA seq data (w5 p.i.) was mined for genes associated with this subset in LCMV and cancer models (Table S2). As shown in Figure 3 G, the expression pattern of multiple genes, including Tcf7, Bach2, Lef1, and Cxcr5 further establish the close relationship with the stem-like subset described in other models (29). However, our data also differ from other systems as the expression of Pdcd1 (which encodes PD1) and Lag3 genes are higher in pop2 than pop3. Additionally, flow cytometry analysis of TCF1 (encoded by Tcf7) and Ly108, both typically increased in stem-like CD8 T cells (29), are also upregulated in pop3 (Fig. 3H). In an LCMV or cancer model, TIM3 expression by stem-like CD8 T cells is a sign of terminal differentiation (30), yet our data show that, although increased in pop3 as compared to pop1 and 2, the levels are lower than in pop4 (Fig. 3H). These findings demonstrate that, during chronic toxoplasma infection, pop3, with strong similarities to stem-like CD8 T cells reported in chronic viral infections and cancer, is the only subset that can transition into all other populations.

Memory CD8 T cell subsets display differential levels of inhibitory receptor expression

Studies from our laboratory have reported that similar to other systems, CD8 T cells from *T. gondii* infected mice show increased expression of inhibitory receptors like PD-1 during the chronic phase of the infection (27). In the present study, we observed that three memory ($CD127^{hi}$) subsets (pop2-4) display higher expression of several inhibitory receptors (PD-1, TIGIT, LAG-3, 2B4, TIM-3, and CTLA-4) as compared to pop1 (Fig. 4A). Unlike RNA sequencing analysis, pop3 exhibits similar levels of PD-1 as pop2 by flow cytometry. The observed discrepancy in PD1 and TIM-3 expression between the RNA sequencing and flow cytometry data can be attributed to the reported limited correlation between mRNA and protein abundance in CD8 T cells (31). This inconsistency can be caused by differences in genetic variations, transcriptional rates, mRNA stability, and rate of protein synthesis and/or

degradation. Moreover, pop3 and pop4 manifest significantly higher expression of TIM-3, TIGIT, TIM3, 2B4, and CTLA-4 than pop2, and co-expression of multiple inhibitory receptors in these two populations is also elevated (Fig. 4B). As previously reported (32), an increase in PD-1 levels in pop2-4 was observed as early as two weeks p.i. (Fig. 4C), however, the decrease in the expression at later time points could be attributed to apoptosis of PD-1^{hi} cells. Early expression of inhibitory molecules (PD-1, TIGIT, TIM3, LAG-3, CTLA4, and 2B4) was also observed in CD8 subsets from the brain and liver (Fig. S3A and B). However, expression of different inhibitory receptors by pop2-4 from the brain and liver remains constant except for decreased PD1 (brain and liver) and LAG-3 (liver only) expression.

CD8 T cell dysfunctionality during chronic viral infection has been partially linked to the sustained presence of antigens (33). As replication of *T. gondii* takes place even during the chronic phase (16), the effect of continuous antigen persistence on the CD8 T cell subsets was assessed. To inhibit parasite replication, infected mice were treated with sulfamethoxazole (34) starting at week 6 p.i., and the CD8 T cell response was evaluated 2 weeks later. As shown in Figure S4A, the frequency and numbers of Ag^{+} CD8 T cells are significantly lower when parasite replication is inhibited by antibiotic treatment, and the frequency of pop3 is increased while other populations are slightly reduced (Fig. S4B and C). However, inhibitory receptors expression by pop2-4 is not affected by the treatment except for a significant decrease in TIGIT expression by pop2 (Fig. S4D).

As previously reported, high antigen load early after infection promotes the differentiation of precursor T cells with acquired hallmarks of exhaustion (32). Moreover, a recent study from our laboratory reported that the generation of CD8 T cell memory against *T. gondii* infection is dose-dependent, with the lower dose driving a stronger Ag^{+} CD8 T cell response at week 8 p.i. (35). In the current study, pop1, 2, and 4 cell numbers are increased in mice infected with 2 cysts compared to animals receiving a 10-cyst challenge (Fig. S5A and B). However, there is no difference in inhibitory receptor expression at week 8 p.i. (data not shown) and the frequency of PD-1^{hi} cells is only reduced in pop2 from mice infected with 2 cysts (Fig. S5C). Thus, although a lower dose of infection generates a superior CD8 T cell response, it is not correlated with a decreased expression of inhibitory receptors.

Our data demonstrates that pop3-4 and to a certain extent pop2, exhibit elevated inhibitory receptor expressions starting as early as week 2 p.i. However, this increase in multiple receptor expression is not dependent on the dose of antigen during the priming or the chronic phase of infection.

Pop4, which resembles terminally differentiated CD8 T cell effectors, exhibits enhanced functionality

CD8 T cells, an important source of IFNγ during *T. gondii* infection, are crucial for controlling the dissemination of the parasites and for protection during acute and chronic infection (13). Additionally, cytolytic activity against infected targets is critical, especially during the chronic stages of the infection (27, 36). As expected, all subsets were in cell cycle at week 2 p.i., based on proliferation marker Ki67, (Fig. 5A) and the expansion is significantly reduced during the chronic phase (Fig. 5B and C). Also, pop3 exhibits moderate proliferation compared to the other subsets. However, a fraction of pop4 and stem-like pop3 remains in cell cycle as demonstrated by an increase in Ki67 MFI in the $Ki67^+$ cells at week 8 p.i. (pop3: 2611±69 (w2), 4965±1051(w8) and pop4: 3485±241 (w2), 6220±2000 (w8) ANOVA with Bonferroni post-test: $p<0.01$). In accordance with our RNA sequencing data (Fig. 2F), pop1, 2, and 4 exhibited significantly higher IFNγ production and cytotoxic activity ($CD107^+$) at week 2 p.i., as compared to pop3 (Fig. 5E and F). Interestingly, while there is a reduction in the percentage of bi-functional CD8 T cells within pop1 and 2 at week 8 p.i., pop4 remains cytotoxic and can still produce IFNγ and TNFα (Fig. 5F). The sustained functionality of pop4 during chronic toxoplasma could be attributed to the continued upregulation of several costimulatory molecules (Fig. S6A-B), that are known to play an important role in T cell activation (37). As shown in Figure S6C, pop4 continues to exhibit increased expression of multiple costimulatory molecules even during the later stages of chronic infection. Our data underlines the functional importance of pop4 during chronic infection which, combined with its ability to convert into pop1, could potentially be important for controlling *T. gondii* reactivation in a toxoplasma-driven encephalitis model.

Discussion

Polyfunctional CD8 T cells are critical for controlling *T. gondii*, especially during the chronic phase of the infection (13). However, in an encephalitis model, reactivation of chronic infection attributed to the dysfunctional state of memory CD8 T cells leads to severe encephalitis and host mortality (27). Cues from chronic viral infections and tumor models, where CD8 T cells play a pivotal role in protection, indicate that memory CD8 T cells are a heterogeneous population with different receptor expression, functional potential, migration, and tissue localization (4). As previously reported (15) and based on our data, *T. gondii* CD8 T cell response does not conform to the general T_{CM}/T_{EM} model. Similarly, our populations could not be defined based on CD27 and a glycoform of CD43 as reported in a respiratory viral infection (38). Therefore, the memory CD8 T cell response during the acute and chronic *T. gondii*

infection was characterized using polychromatic flow cytometric analysis. A previously described surrogate marker strategy using CD44 and CD11a has been validated in our model (18, 35, 39) and allows for the investigation of Toxoplasma Ag^+ polyclonal CD8 T cell response with minimal contamination by naïve cells (10% or less) (Fig. 1B). In our study, Ag^+ ($CD11a^{hi}CD44^{hi}$) CD8 T cells can be divided into four subsets based on CD62L and KLRG1 expression. While we used a clustering algorithm to define our populations, Wilson *et al.* had previously used the same markers to study the role of IL-12 in the CTL response against *T. gondii* infection (19). This report demonstrated that CTL cells can be fractionated into a T_{CM} fraction I ($KLRG1^-CD62L^{hi}$), T_{EM} fraction II ($KLRG1^-CD62L^{lo}$), effector cell rich fraction III ($KLRG1^+CD62L^{lo}$), and fraction IV ($KLRG1^+CD62L^{hi}$) during both acute and chronic phases of infection. However, these fractions were not characterized beyond KLRG1 and CD62L expression. Akin to our findings, Wilson *et al.* identified $KLRG1^+CD62L^{lo}$ and $KLRG1^-CD62L^{lo}$ CD8 T cells as the most dominant subsets in the brains of chronically infected mice (19). In our study, pop1 displays the characteristics of terminally differentiated effector CD8 T cells ($KLRG1^+CD62L^{lo}$) with significant increases in molecules associated with cytotoxicity, cytokines, and various annexin and caspases (Fig. 2F). Pop2 ($KLRG1^-CD62L^{lo}$) is similar to T_{EM} with low levels of KLRG1, CD62L, CCR7, and high inhibitory receptor expression. Conversely, pop3 ($KLRG1^-CD62L^{hi}$) expressed high CD62L and TCF7, as well as multiple genes associated with stem-like memory CD8 T cells. Pop4 ($KLRG1^+CD62L^{hi}$) displays an intermediate effector/memory profile.

Similar to the stem-like CD8 T cells in viral and cancer models, pop3 demonstrates increased expression of Tox, Tcf1, Bach2, Lef1, Id3, Slamf6, and Zeb1, as well as genes related to translation, especially those encoding ribosomal proteins that are highly expressed in stem-like CD8 T cells (28). Pop3 also presents an elevated expression of TCF7, CXCR5, CXCR3, and Ly108. More importantly, adoptive transfer studies demonstrate that pop3 can retain its phenotype when transferred to equally infected mice but also convert into pop2, pop4, and possibly pop1 when transferred to naïve mice that were subsequently challenged. Stem-like CD8 T cells have been extensively studied in LCMV and cancer models where this self-renewing $PD\text{-}1^+$ $TCF\text{-}1^+$ population contributes to the maintenance of robust T cell immunity under chronic antigenic stimulation (11, 30). Due to their long-term persistence and ability to transition into different subsets, stem-like CD8 T cells are considered ideal targets for cancer immunotherapy. These cells are responsive to PD-1 blockade that accelerates their differentiation into an effector population (40). As previously demonstrated by our laboratory,

CD8 T cells can be rescued by anti-PDL-1 treatment (27), thus, it is likely that the stem-like population plays a critical role in controlling the reactivation of chronic *T. gondii* infection.

Interestingly, pop4, which can be derived from pop3, retains a commonality with parental stem-like memory subset based on the expression of surface markers like CD127, CCR7, and CD27. However, when adoptively transferred, the majority of pop4 transitioned into pop1 and these two populations differ only by 43 DEGs with Sell (which encodes CD62L) being the most dysregulated gene. Notably, pop4 displays some of the attributes of both effector ($KLRG1^+$) and memory ($CD127^{hi}$) CD8 T cells akin to the hybrid effector-memory phenotype described by Chu *et al* in a resistant model of chronic toxoplasmosis (15). In this study, $CXCR3^-KLRG1^-$ CD8 T cells were identified as effector CD8 T cells, $CXCR3^+KLRG1^-$ as a memory subset, and $CXCR3^+KLRG1^+$ as an intermediate effector/memory population with antigen-dependent maintenance. In our model, based on CXCR3 and KLRG1 expression by the different populations, pop2 and pop3 resemble the $CXCR3^+KLRG1^-$ subset while pop4 bears a striking likeness to the intermediate $CXCR3^+KLRG1^+$ population (15). However, unlike our findings, none of the subsets described in this report expressed CD62L or CCR7. Interestingly, in our study, not only does pop4 exhibit a significantly higher frequency of $IFN\gamma^+CD107a^+$ than pop1 as early as week 2 p.i., but this continued functionality, associated with lower inhibitory receptors and higher costimulatory molecules expression, underlines the potentially critical role of pop4 over a more traditional effector population. Our data, combined with the earlier report from Chu *et al* (15) in a resistant model of *T. gondii* infection indicates that this intermediate effector/memory population could play an important role in long-term immunity against the parasite.

Overall, the CD8 T cell memory response during chronic toxoplasmosis in an encephalitis model appears to be a complex process with multiple subsets playing distinct roles throughout the infection. Recently, a consensus seems to have emerged, and different subsets were defined as exhausted progenitor CD8 T cells (Tex^{prog}/T_{pex}), terminally differentiated exhausted (Tex^{term}/T_{ex}), terminally differentiated effector (Tex^{eff}/T_{eff}), and exhausted hybrid phenotype (Tex^{int}/T_{int})(11, 41). During chronic toxoplasmosis, pop3 displays stem-like characteristics that resemble the TCF-1^{hi} self-renewing Tex^{prog} (T_{pex}) and due to its plasticity can be an important source of effector (pop1) and memory subsets (pop 2 and pop4). Similarly, pop2 exhibits some of the features of Tex^{term} (T_{ex}) with elevated exhaustion signature and reduced functionality. However, pop2 may not be terminally differentiated as this subset can convert into pop1 which manifests similarity to Tex^{eff} (T_{eff}). Interestingly, pop4 which resembles Tex^{int} (T_{int}) is also able

to transition into pop1. The major difference between TCF1^{hi} Tim3^{hi} pop4, and the Tex^{int} (T_{int}) population described in cancer and viral infections, is the absence of an exhausted phenotype correlated with the maintenance of a strong functional fitness even at later stages of chronic infection (41). Understandably, the infection dynamics between viral and parasitic pathogens are different, and further studies are required to characterize in-depth variations between the memory subsets generated in chronic viral versus toxoplasma infection. Our results raise several important questions, and the answers are essential for understanding the plasticity of the different memory populations generated during chronic *T. gondii* infection and may provide insights into CD8 T cell immunity to other non-viral infections. For example, discerning why pop4, which exhibits better functionality, is converting into a less functional pop1 and the reason for the maintenance of this suboptimal effector population during chronic infection should be further investigated. Moreover, the discrepancy between the subsets described in our study and other models suggests that the composition of the populations may be more complex, and further characterization may be necessary.

Materials and Methods

Mice and parasites.

C57BL6/J and B6-Ly5.2 (CD45.1) mice were purchased from The Jackson Laboratory and housed in a specific pathogen-free facility at The George Washington University. All experiments were performed per institutional policies and regulations of the relevant animal welfare acts and have been reviewed and approved by The George Washington University institutional animal care and use committee. *T. gondii* cysts of the Me49 strain were isolated from the brains of infected CBA/J mice at 5 weeks post-infection. Six to eight-week-old mice were infected via the intragastric route with 10 cysts unless otherwise stated. Mice were sacrificed by CO2 inhalation at different time points post-infection. *T. gondii* lysate antigen (TLA) was prepared from the RH strain of *T. gondii* as previously described (18). Toxoplasma-infected mice (6 weeks p.i.) were administered sulfamethoxazole (800 mg/l) in drinking water for 2 weeks (34), and medicated water was replaced every third day.

Lymphocyte isolation and staining.

Single-cell suspension was prepared from the spleen, liver, blood, and brain of mice using standard protocols (18). Surface staining was performed for 20 minutes at 4^0C in PBS supplemented with 2% bovine calf serum with the following antibodies: CD8 (YTS156.7.7), CD11a (M17/4), CD44 (IM7), CD62L (MEL-14), KLRG1 (2F1), CD43 (1B11), CD27 (LG.3A10), CCR7 (4B12), CX3CR1 (SA011F11), CXCR5 (L128D7), CXCR3 (CXCR3-173), CTLA-4 (UC10-4B9), TIGIT (1G9), 2B4 (m2B4(B6)458.1, TIM3 (RMT3-23), LAG-3 (C9B7W), PD-1

(RMP1-30), CD28 (37.51), OX40 (OX-86), CD40L (MR1), GITR (DTA-1), CD45.1 (A20), CD45.2 (104), IFNγ (XMG1.2) were purchased from Biolegend and CD127 (A7R34), CD27 (LG.7F9), 41BB (17B5), ICOS (7E.17G9), Ly108 (13G3-19D), TNFα (MP6-XT22), and Ki67 (SolA15) from Thermofisher Scientific. Anti TCF1 (C63D9) was purchased from Cell Signaling. Tgd057 tetramers were obtained for the NIH tetramer facility (Atlanta, GA). Tetramer staining was performed at 4^0C for 1 hour in PBS supplemented with bovine calf serum. For cytokine detection, lymphocytes were stimulated for 18 hours with 30µg/ml of TLA, and Protein Transport Inhibitor Cocktail (eBioscience, Thermofisher Scientific) was added during the last 4 hours of restimulation. After surface staining and permeabilization/fixation (IC Fixation buffer, Thermofisher Scientific), cells were stained for intracellular cytokine detection as previously described (18). Intracellular staining for transcription factor detection was performed after permeabilization and fixation using Cytofix/Cytoperm kit (BD Biosciences). Data were acquired with a BD FACSCelesta or LSR Fortessa and analyzed with FlowJo software (BD Biosciences). Dead cells were systematically excluded using the LIVE/DEAD fixable aqua dead cell stain kit (ThermoFisher Scientific), and quality control was performed with FlowAI (FlowJo). Co-expression analysis was performed with SPICE 6 (42). Multiparametric flow cytometry data were analyzed and visualized with FlowSOM and TriMap dimensionality reduction algorithms.

Adoptive transfer.

CD8 T cells were purified from spleens of CD45.1 infected mice using the EasySep Mouse CD8 T cell isolation kit (Stemcell Technologies). The enriched CD8 cell suspension was then labeled with fluorescent antibodies (CD8, CD11a, CD44, CD62L, and KLRG1), and the different populations were then sorted with a BD Influx cell sorter (purity ≥90%). Dead cells were excluded using Sytox Blue (ThermoFisher Scientific). Cells from each population were individually transferred to infected or naïve CD45.2 mice (10^5 cells/mouse) via tail vein injection. Naïve mice injected with cells were challenged the next day with *T. gondii* (10 cysts/mouse) via intragastric route.

RNA extraction, sequencing, and analysis.

RNA extraction from sorted CD8 T cell populations pooled from 5-7 mice (week 5 and 8 p.i.) was performed using the RNeasy Plus mini kit (Qiagen) following the manufacturer's protocol. Each sample group was comprised of two experimental replicates. Ribosomal RNA was removed using a NEBNext rRNA Depletion kit, followed by library preparation with NEBNext Ultra II RNA Library Preparation kit for Illumina (New England BioLabs). Samples were sequenced by Genewiz (Azenta Life Sciences) on an Illumina HiSeq platform with 2x150 bp sequencing read length. RNAseq data are available in the GEO database (accession

GSE280150). RNA-seq analysis was performed using Galaxy (43). After quality control and adapter sequences trimming (Cutadapt Galaxy version 4.7+galaxy0) (44), the remaining rRNA was removed using SortMeRNA (Galaxy version 2.1b.6)(45). Reads were mapped to the mouse genome (GRCm38/mm10) using RNA STAR (Galaxy version 2.7.11a+galaxy0) (46). GC bias was evaluated with computeGCBias (Galaxy version 3.5.4+galaxy0) and corrected when needed using correctGCBias (Galaxy version 3.5.4+galaxy0) (47). Transcripts were quantified using featureCounts (Galaxy version 2.0.3+galaxy2)(48), and differential gene expression analysis was performed using DESeq2 (Galaxy version 2.11.40.8+galaxy0)(49). Genes were considered differentially expressed if they achieved an adjusted p-value <0.05 and |log2 fold change| >1. PCA was generated from VST-normalized counts using PCA plot w ggplot2 (Galaxy version 3.4.0+galaxy0) (50). The volcano plot and Venn diagram were generated in Galaxy (Galaxy version 0.0.5 and Galaxy version 0.1.1, respectively). Spearman's Correlation Coefficient plot was generated with log-transformed normalized count data generated by DESeq2. The top 3800+ DEGs among the four populations (pop1-4) were selected for further analysis and divided into 6 clusters by K-means clustering (numeric clustering, Galaxy version 1.0.11.0). The data was visualized with heatmaps using the z-scores and log2(+1)-transformed normalized counts. Overrepresented gene ontology categories were determined with Metascape (https://metascape.org)(51). Spearman's correlation and heatmap were visualized using GraphPad Prism (Version 10.2.2).

Statistical analysis

Differences in percentage, absolute number, and MFI for each experiment were assessed using one-way ANOVA with Bonferroni post-test. Error bars in the graph indicate the SEM of values from individual mice. All computations were completed using GraphPad Prism software.

Acknowledgments

We thank Gregory Cresswell and the Flow Cytometry Core Facility at George Washington University for assistance with sorting of the CD8 T cell subsets. The core is supported by the George Washington University Cancer Center and School of Medicine and Health Sciences.

References

1. V. Kalia, S. Sarkar, R. Ahmed, CD8 T-cell memory differentiation during acute and chronic viral infections. *Adv Exp Med Biol* **684**, 79-95 (2010).
2. H. Raskov, A. Orhan, J. P. Christensen, I. Gogenur, Cytotoxic CD8(+) T cells in cancer and cancer immunotherapy. *Br J Cancer* **124**, 359-367 (2021).

3. Y. Yuzefpolskiy, F. M. Baumann, V. Kalia, S. Sarkar, Early CD8 T-cell memory precursors and terminal effectors exhibit equipotent in vivo degranulation. *Cell Mol Immunol* **12**, 400-408 (2015).
4. W. Cui, S. M. Kaech, Generation of effector CD8+ T cells and their conversion to memory T cells. *Immunol Rev* **236**, 151-166 (2010).
5. C. R. Plumlee *et al.*, Early Effector CD8 T Cells Display Plasticity in Populating the Short-Lived Effector and Memory-Precursor Pools Following Bacterial or Viral Infection. *Sci Rep* **5**, 12264 (2015).
6. M. D. Martin, V. P. Badovinac, Defining Memory CD8 T Cell. *Front Immunol* **9**, 2692 (2018).
7. F. Sallusto, J. Geginat, A. Lanzavecchia, Central memory and effector memory T cell subsets: function, generation, and maintenance. *Annu Rev Immunol* **22**, 745-763 (2004).
8. F. R. Carbone, Unique properties of tissue-resident memory T cells in the lungs: implications for COVID-19 and other respiratory diseases. *Nat Rev Immunol* **23**, 329-335 (2023).
9. R. Zander, W. Cui, Exhausted CD8(+) T cells face a developmental fork in the road. *Trends Immunol* **44**, 276-286 (2023).
10. M. Ando, M. Ito, T. Srirat, T. Kondo, A. Yoshimura, Memory T cell, exhaustion, and tumor immunity. *Immunol Med* **43**, 1-9 (2020).
11. T. Gebhardt, S. L. Park, I. A. Parish, Stem-like exhausted and memory CD8(+) T cells in cancer. *Nat Rev Cancer* **23**, 780-798 (2023).
12. H. Bisetegn *et al.*, Global seroprevalence of Toxoplasma gondii infection among patients with mental and neurological disorders: A systematic review and meta-analysis. *Health Sci Rep* **6**, e1319 (2023).
13. R. Bhadra, J. P. Gigley, I. A. Khan, The CD8 T-cell road to immunotherapy of toxoplasmosis. *Immunotherapy* **3**, 789-801 (2011).
14. G. P. Brandao *et al.*, Susceptibility to re-infection in C57BL/6 mice with recombinant strains of Toxoplasma gondii. *Exp Parasitol* **128**, 433-437 (2011).
15. H. H. Chu *et al.*, Continuous Effector CD8(+) T Cell Production in a Controlled Persistent Infection Is Sustained by a Proliferative Intermediate Population. *Immunity* **45**, 159-171 (2016).
16. E. Watts *et al.*, Novel Approaches Reveal that Toxoplasma gondii Bradyzoites within Tissue Cysts Are Dynamic and Replicating Entities In Vivo. *mBio* **6**, e01155-01115 (2015).
17. D. Masopust, K. Murali-Krishna, R. Ahmed, Quantitating the magnitude of the lymphocytic choriomeningitis virus-specific CD8 T-cell response: it is even bigger than we thought. *J Virol* **81**, 2002-2011 (2007).
18. S. Hwang, D. A. Cobb, R. Bhadra, B. Youngblood, I. A. Khan, Blimp-1-mediated CD4 T cell exhaustion causes CD8 T cell dysfunction during chronic toxoplasmosis. *J Exp Med* **213**, 1799-1818 (2016).
19. D. C. Wilson *et al.*, Differential regulation of effector- and central-memory responses to Toxoplasma gondii Infection by IL-12 revealed by tracking of Tgd057-specific CD8+ T cells. *PLoS Pathog* **6**, e1000815 (2010).
20. K. R. Renkema *et al.*, KLRG1(+) Memory CD8 T Cells Combine Properties of Short-Lived Effectors and Long-Lived Memory. *J Immunol* **205**, 1059-1069 (2020).
21. J. J. Obar, L. Lefrancois, Early signals during CD8 T cell priming regulate the generation of central memory cells. *J Immunol* **185**, 263-272 (2010).

22. J. A. Olson, C. McDonald-Hyman, S. C. Jameson, S. E. Hamilton, Effector-like CD8(+) T cells in the memory population mediate potent protective immunity. *Immunity* **38**, 1250-1260 (2013).
23. A. F. Ochsenbein *et al.*, CD27 expression promotes long-term survival of functional effector-memory CD8+ cytotoxic T lymphocytes in HIV-infected patients. *J Exp Med* **200**, 1407-1417 (2004).
24. J. P. Bottcher *et al.*, Functional classification of memory CD8(+) T cells by CX3CR1 expression. *Nat Commun* **6**, 8306 (2015).
25. D. J. Bangs *et al.*, CXCR3 regulates stem and proliferative CD8+ T cells during chronic infection by promoting interactions with DCs in splenic bridging channels. *Cell Rep* **38**, 110266 (2022).
26. K. M. Valentine, K. K. Hoyer, CXCR5+ CD8 T Cells: Protective or Pathogenic? *Front Immunol* **10**, 1322 (2019).
27. R. Bhadra, J. P. Gigley, L. M. Weiss, I. A. Khan, Control of Toxoplasma reactivation by rescue of dysfunctional CD8+ T-cell response via PD-1-PDL-1 blockade. *Proc Natl Acad Sci U S A* **108**, 9196-9201 (2011).
28. S. Ando *et al.*, mTOR regulates T cell exhaustion and PD-1-targeted immunotherapy response during chronic viral infection. *J Clin Invest* **133** (2023).
29. D. Zehn, R. Thimme, E. Lugli, G. P. de Almeida, A. Oxenius, 'Stem-like' precursors are the fount to sustain persistent CD8(+) T cell responses. *Nat Immunol* **23**, 836-847 (2022).
30. S. J. Im *et al.*, Characteristics and anatomic location of PD-1(+)TCF1(+) stem-like CD8 T cells in chronic viral infection and cancer. *Proc Natl Acad Sci U S A* **120**, e2221985120 (2023).
31. B. P. Nicolet, M. C. Wolkers, The relationship of mRNA with protein expression in CD8+ T cells associates with gene class and gene characteristics. *PLoS One* **17**, e0276294 (2022).
32. E. Ahn *et al.*, Role of PD-1 during effector CD8 T cell differentiation. *Proc Natl Acad Sci U S A* **115**, 4749-4754 (2018).
33. E. I. Zuniga, J. A. Harker, T-cell exhaustion due to persistent antigen: quantity not quality? *Eur J Immunol* **42**, 2285-2289 (2012).
34. C. Jost, I. Reiter-Owona, O. Liesenfeld, The timing of sulfadiazine therapy impacts the reactivation of latent Toxoplasma infection in IRF-8-/- mice. *Parasitol Res* **101**, 1603-1609 (2007).
35. M. M. Moretto, J. Chen, M. Meador, J. Phan, I. A. Khan, A Lower Dose of Infection Generates a Better Long-Term Immune Response against Toxoplasma gondii. *Immunohorizons* **7**, 177-190 (2023).
36. E. Y. Denkers *et al.*, Perforin-mediated cytolysis plays a limited role in host resistance to Toxoplasma gondii. *J Immunol* **159**, 1903-1908 (1997).
37. P. A. Duttagupta, A. C. Boesteanu, P. D. Katsikis, Costimulation signals for memory CD8+ T cells during viral infections. *Crit Rev Immunol* **29**, 469-486 (2009).
38. H. Hikono *et al.*, Activation phenotype, rather than central- or effector-memory phenotype, predicts the recall efficacy of memory CD8+ T cells. *J Exp Med* **204**, 1625-1636 (2007).
39. D. Rai, N. L. Pham, J. T. Harty, V. P. Badovinac, Tracking the total CD8 T cell response to infection reveals substantial discordance in magnitude and kinetics between inbred and outbred hosts. *J Immunol* **183**, 7672-7681 (2009).

40. A. L. Gill *et al.*, PD-1 blockade increases the self-renewal of stem-like CD8 T cells to compensate for their accelerated differentiation into effectors. *Sci Immunol* **8**, eadg0539 (2023).
41. M. K. Rahim *et al.*, Dynamic CD8(+) T cell responses to cancer immunotherapy in human regional lymph nodes are disrupted in metastatic lymph nodes. *Cell* **186**, 1127-1143 e1118 (2023).
42. M. Roederer, A proposal for unified flow cytometer parameter naming. *Cytometry A* **87**, 689-691 (2015).
43. E. Afgan *et al.*, The Galaxy platform for accessible, reproducible and collaborative biomedical analyses: 2018 update. *Nucleic Acids Res* **46**, W537-W544 (2018).
44. M. Martin, Cutadapt Removes Adapter Sequences From High-Throughput Sequencing Reads. *EMBnet.journal* **17**, 10-12 (2011).
45. E. Kopylova, L. Noe, H. Touzet, SortMeRNA: fast and accurate filtering of ribosomal RNAs in metatranscriptomic data. *Bioinformatics* **28**, 3211-3217 (2012).
46. A. Dobin *et al.*, STAR: ultrafast universal RNA-seq aligner. *Bioinformatics* **29**, 15-21 (2013).
47. F. Ramirez *et al.*, deepTools2: a next generation web server for deep-sequencing data analysis. *Nucleic Acids Res* **44**, W160-165 (2016).
48. Y. Liao, G. K. Smyth, W. Shi, featureCounts: an efficient general purpose program for assigning sequence reads to genomic features. *Bioinformatics* **30**, 923-930 (2014).
49. M. I. Love, W. Huber, S. Anders, Moderated estimation of fold change and dispersion for RNA-seq data with DESeq2. *Genome Biol* **15**, 550 (2014).
50. H. Wickham, "ggplot2: Elegant Graphics for Data Analysis". (Springer-Verlag, New York, 2016).
51. Y. Zhou *et al.*, Metascape provides a biologist-oriented resource for the analysis of systems-level datasets. *Nat Commun* **10**, 1523 (2019).

Figures and Tables

Figure 1. Phenotypic characterization of CD8 T cell subsets after *T. gondii* infection.

C57BL6/J mice were infected with 10 cysts of *T. gondii* (strain Me49) via oral route. A) FlowSOM minimal spanning tree of Ag^+ ($CD44^{hi}CD11a^{hi}$) CD8 T cells from the spleen using CD127, CD62L, CCR7, and KLRG1 at week 5 p.i. B-C) KLRG1 (B) and CD62L (C) overlay on the clustering tree. D) Four populations characterized by KLRG1 and CD62L expression (gated on Ag^+ CD8 T cells) at week 5 p.i. (pop1: $KLRG1^+CD62L^{lo}$, pop2: $KLRG1^-CD62L^{lo}$, pop3: $KLRG1^-CD62L^{hi}$, pop4: $KLRG1^+CD62L^{hi}$). E) TriMap representation of CD127, CCR7, CD62L, and KLRG1 expression by Ag^+ CD8 T cells at week 5 p.i. F) Pop1-4 overlay on the TriMap representation at week 5 p.i. G) Frequency and number of cells for pop1-4 in the spleen at week 5 p.i. H) Kinetic of Ag^+ and pop1-4 cell numbers at week 2, 5, and 8 p.i. I) Geometric MFI (gMFI) of CD127, CCR7, CD27, CD43 by pop1-4 at week 5 p.i. J) gMFI of CX3CR1, CXCR5, and CXCR3 for pop1-4 at week 5 p.i. K) Heatmap of CD127, CCR7, CD27, CD43, CX3CR1, CXCR5, and CXCR3 gMFI for pop1-4 at week 5 p.i. I, J: Numbers on histograms represent the gMFI±SEM of each marker in the four populations.

G-H: Data presented as mean of individual mice ± SEM compiled from at least 3 experiments. *p<0.05, **p<0.01, and ****p<0.001 (one-way ANOVA with Bonferroni post-test).

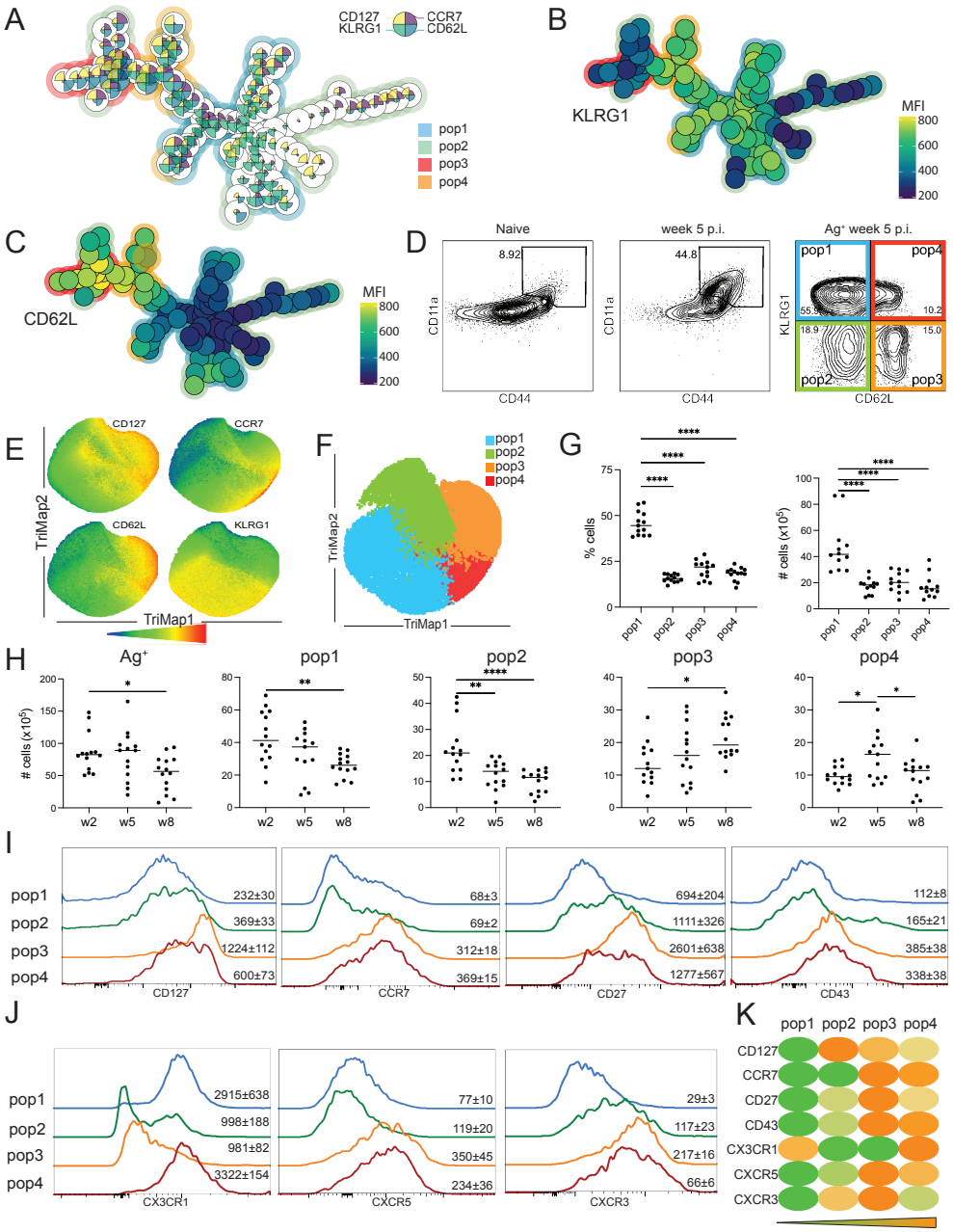

Figure 2. Transcriptomic analysis of CD8 T cell subsets defines four individual populations.

C57BL6/J mice were infected with 10 cysts of *T. gondii* (strain Me49) via oral route. At week 8 p.i., CD8 subsets were sorted from the spleen, and RNAseq was performed. A) Principal Component Analysis. B) Heatmap illustrating Spearman's correlation among individual samples. C) Venn diagram for DEGs from pop1, pop3, and pop4. D) Heatmap showing the relative expression of the 43 DEGs dysregulated between pop1 and pop4 at w8. Genes were divided into clusters by K-mean clustering based on expression. E) Volcano plot of the 43 DEGs in pop4 compared to pop1. F) Heatmap showing the relative expression of DEGs between the four populations at w8. Genes were divided into clusters by K-mean clustering based on expression. G) Metascape analysis indicating the biological processes associated with genes in the clusters defined in (F). Data are from two independent experiments with samples pooled from 5-7 mice for sorting individual populations.

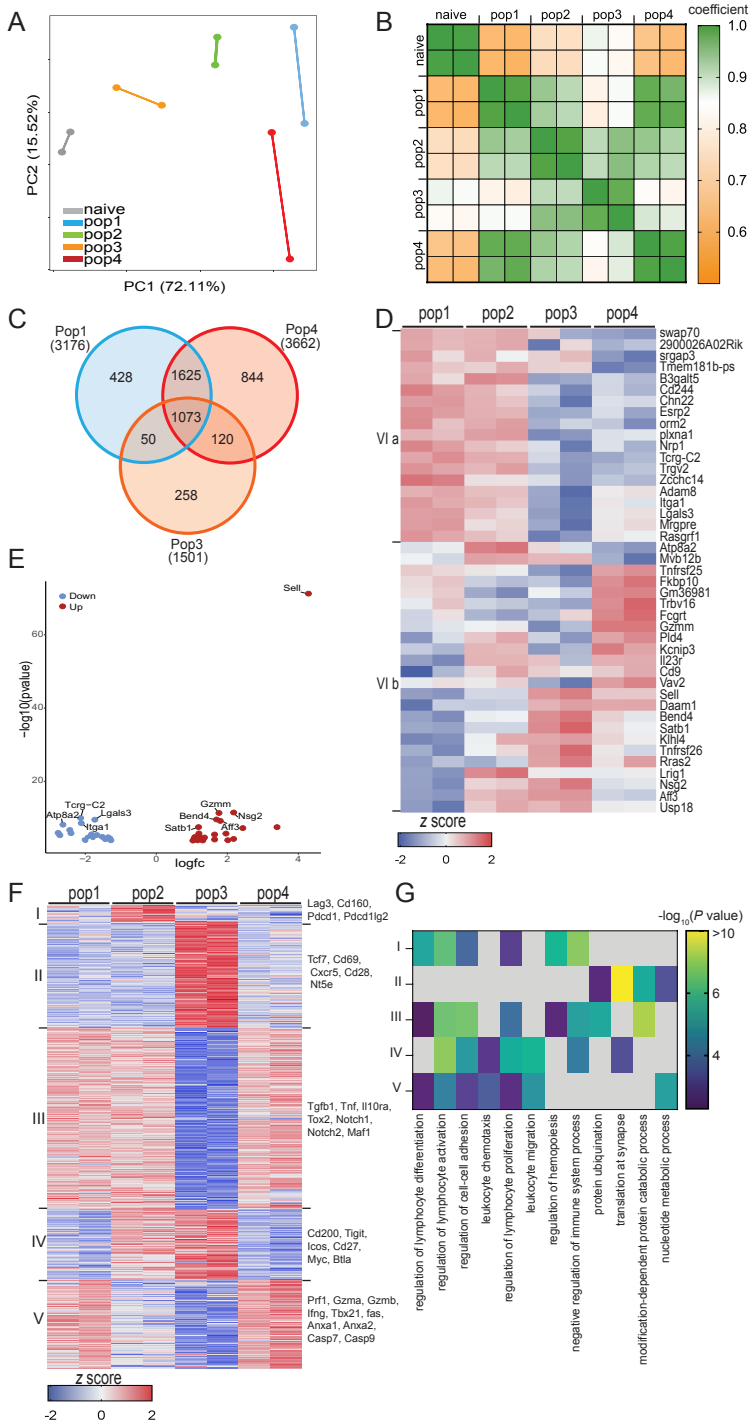
A
PC2 (15.52%)
PC1 (72.11%)
naive
pop1
pop2
pop3
pop4
B
naive
pop1
pop2
pop3
pop4
coefficient
1.0
0.9
0.8
0.7
0.6
C
Pop1
(3176)
Pop4
(3662)
Pop3
(1501)
428
1625
844
1073
50
120
258
D
pop1
pop2
pop3
pop4
VI a
VI b
swap70
2900026A02Rik
srgap3
Tmem181b-ps
B3galt5
Cd244
Chn22
Esrp2
orm2
plxna1
Nrp1
Tcrg-C2
Trgv2
Zcchc14
Adam8
Itga1
Lgals3
Mrgpre
Rasgrf1
Atp8a2
Mvb12b
Tnfrsf25
Fkbp10
Gm36981
Trbv16
Fcgrt
Gzmm
Pld4
Kcnip3
Il23r
Cd9
Vav2
Sell
Daam1
Bend4
Satb1
Klhl4
Tnfrsf26
Rtras2
Lrig1
Nsg2
Aff3
Usp18
z score
-2
0
2
E
Down
Up
Sell
-log10(pvalue)
logfc
Tcrg-C2
Atp8a2
Lgals3
Itga1
Gzmm
Bend4
Nsg2
Satb1
Aff3
F
pop1
pop2
pop3
pop4
I
II
III
IV
V
Lag3, Cd160,
Pdcd1, Pdcd1lg2
Tcf7, Cd69,
Cxcr5, Cd28,
Nt5e
Tgfb1, Tnf, Il10ra,
Tox2, Notch1,
Notch2, Maf1
Cd200, Tigit,
Icos, Cd27,
Myc, Btla
Prf1, Gzma, Gzmb,
Ifng, Tbx21, fas,
Anxa1, Anxa2,
Casp7, Casp9
z score
-2
0
2
G
-log10(P value)
>10
6
4
regulation of lymphocyte differentiation
regulation of lymphocyte activation
regulation of cell-cell adhesion
leukocyte chemotaxis
regulation of lymphocyte proliferation
leukocyte migration
regulation of hemopoiesis
negative regulation of immune system process
protein ubiquination
translation at synapse
modification-dependent protein catabolic process
nucleotide metabolic process

Figure 3. Memory CD8 T cell subsets exhibit plasticity when transferred to equally infected or naïve mice.

A) Schematic for adoptive transfer of pop1-4 from 5 weeks infected CD45.1 mice to similarly infected CD45.2 animals. B) Number of CD45.1 cells recovered from the spleen of recipients at 6 days post-transfer. C) Phenotype of transferred cells recovered from each group of recipients (pop1-pop4 from left to right) presented as the frequency of CD45.1 cells. D) Schematic for adoptive transfer of pop1-4 from week 5 infected CD45.1 mice to naïve CD45.1 animals. Recipients were challenged one day post-transfer. E) Number of CD45.1 cells recovered from the spleen of recipients at day 15 p.i. F) Phenotype of transferred cells recovered from each group of recipients (pop1-pop4 from left to right) presented as the frequency of CD45.1 cells. G) Heatmap of differentially expressed genes associated with stem-like CD8 T cells in pop1-4 at week 5 p.i. H) gMFI of TCF-1 and Ly108 at week 5 p.i. B, C, E, F, and H: Data presented as mean from individual mice ± SEM compiled from 2 experiments. *$p<0.05$, ***$p\leq0.001$, and ****$p<0.001$ (one-way ANOVA with Bonferroni post-test).

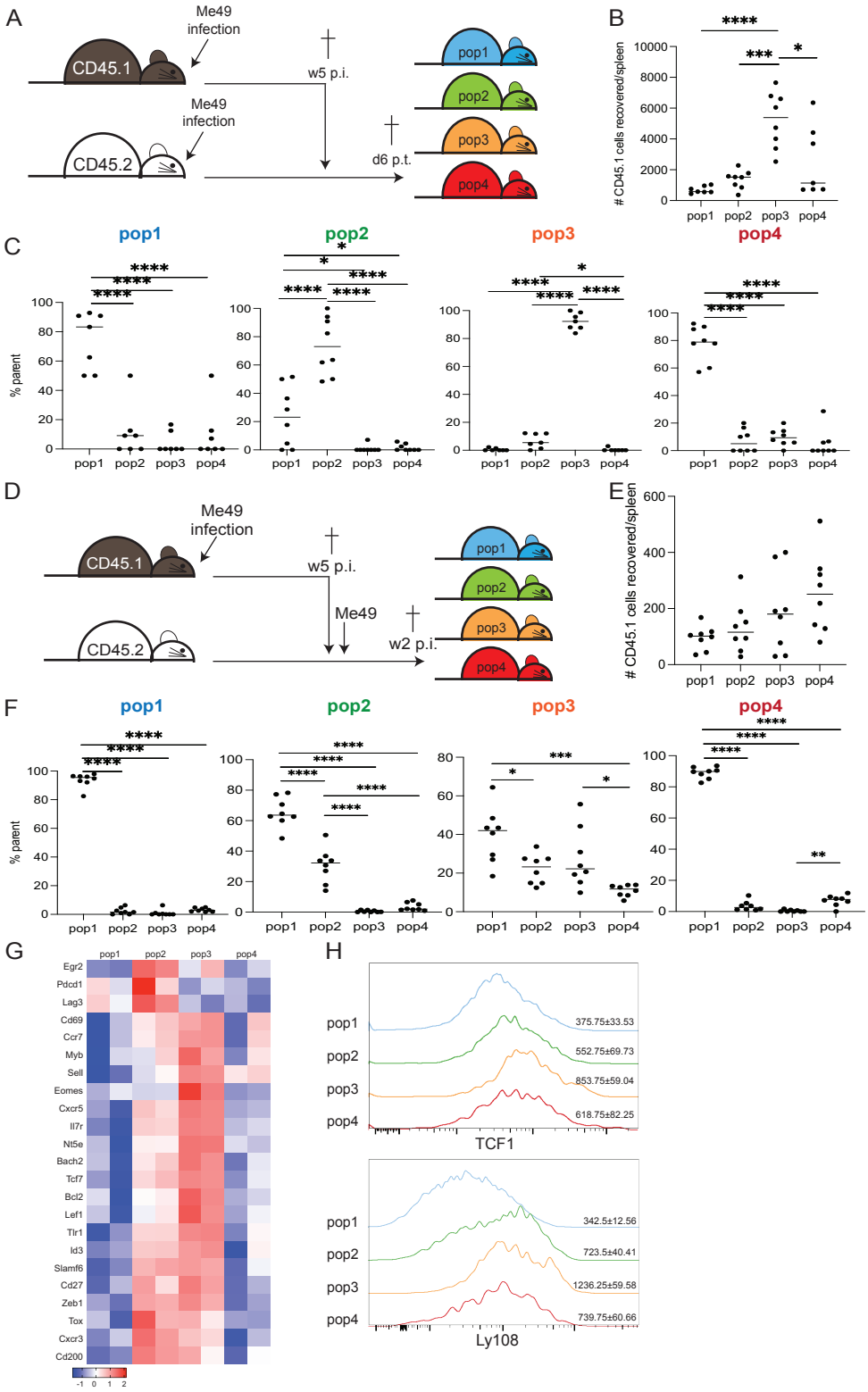
A
Me49 infection
CD45.1
w5 p.i.
Me49 infection
CD45.2
d6 p.t.
pop1
pop2
pop3
pop4
B
CD45.1 cells recovered/spleen
C
% parent
D
Me49 infection
CD45.1
w5 p.i.
Me49
CD45.2
w2 p.i.
E
CD45.1 cells recovered/spleen
F
% parent
G
Egr2
Pdcd1
Lag3
Cd69
Ccr7
Myb
Sell
Eomes
Cxcr5
Il7r
Nt5e
Bach2
Tcf7
Bcl2
Lef1
Tlr1
Id3
Slamf6
Cd27
Zeb1
Tox
Cxcr3
Cd200
H
375.75±33.53
552.75±69.73
853.75±59.04
618.75±82.25
TCF1
342.5±12.56
723.5±40.41
1236.25±59.58
739.75±60.66
Ly108

Figure 4. Stem-like memory CD8 subset (pop3) exhibits high multiple inhibitory receptor expression.

A) Expression of PD1, TIGIT, LAG-3, 2B4, TIM3, and CTLA4 by pop1-4 from the spleen at week 8 p.i. Numbers on histograms represent gMFI ± SEM of each marker in the four populations and CD8 T cells from naïve mice. B) Co-expression of multiple inhibitory receptors (PD1, TIGIT, LAG-3, 2B4, TIM3, and CTLA4) for pop1-4 at week 8 p.i. using SPICE. C) Kinetics of PD-1, TIGIT, LAG-3, 2B4, TIM3, and CTLA4 expression for pop2-4. MFI for individual mice is representative of 3 independent experiments. *$p<0.05$, **$p<0.01$, ***$p\leq0.001$, and ****$p<0.001$ (one-way ANOVA with Bonferroni post-test).

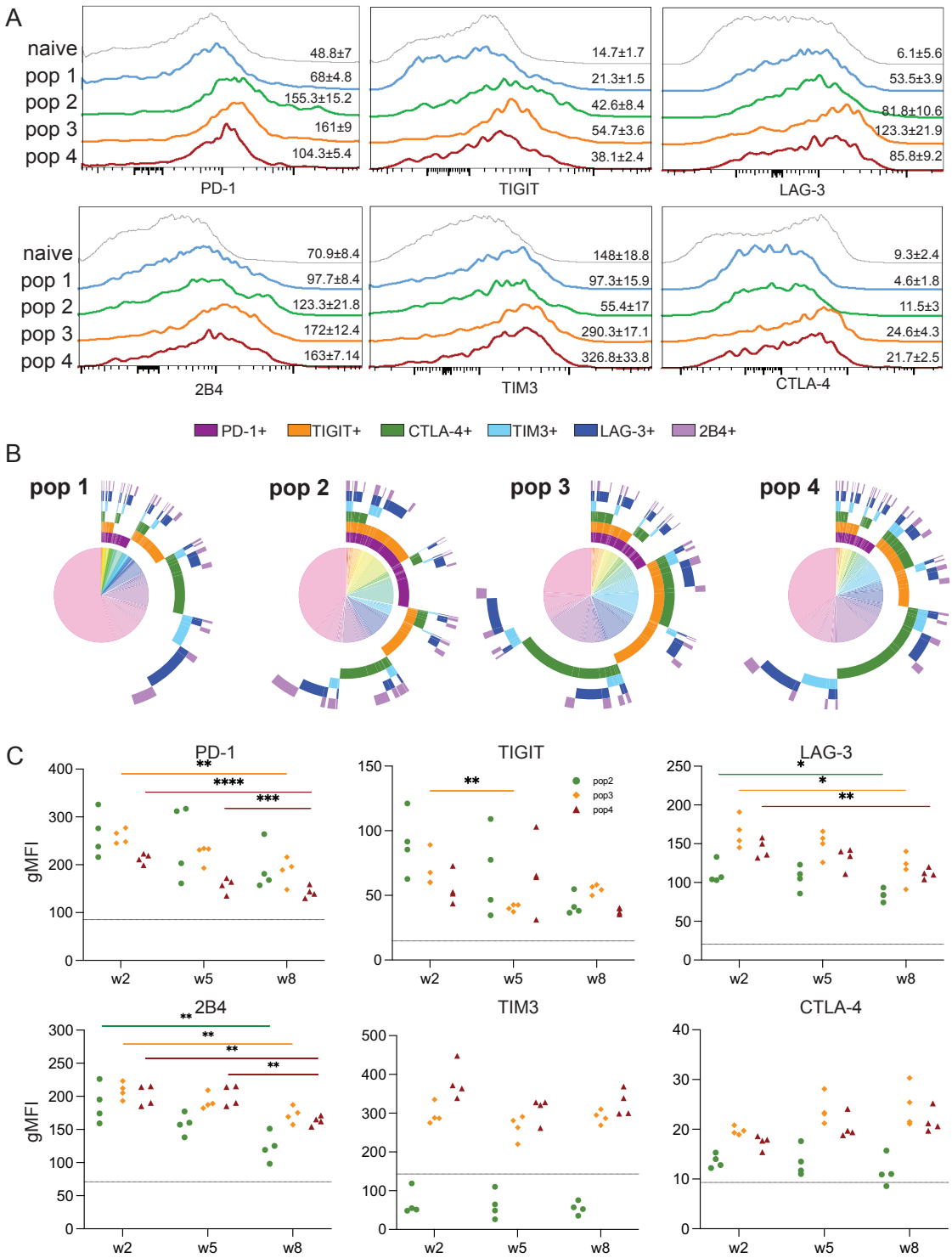
A
naive
pop 1
pop 2
pop 3
pop 4
48.8±7
68±4.8
155.3±15.2
161±9
104.3±5.4
PD-1
14.7±1.7
21.3±1.5
42.6±8.4
54.7±3.6
38.1±2.4
TIGIT
6.1±5.6
53.5±3.9
81.8±10.6
123.3±21.9
85.8±9.2
LAG-3
70.9±8.4
97.7±8.4
123.3±21.8
172±12.4
163±7.14
2B4
148±18.8
97.3±15.9
55.4±17
290.3±17.1
326.8±33.8
TIM3
9.3±2.4
4.6±1.8
11.5±3
24.6±4.3
21.7±2.5
CTLA-4
PD-1+
TIGIT+
CTLA-4+
TIM3+
LAG-3+
2B4+
B
pop 1
pop 2
pop 3
pop 4
C
PD-1
TIGIT
LAG-3
2B4
TIM3
CTLA-4
gMFI
pop2
pop3
pop4
w2
w5
w8

Figure 5. Pop4 maintains elevated functional fitness during chronic *T. gondii* infection.

A) Ki67 expression for pop1-4 from spleen of infected mice at week 2 p.i. and 8 p.i., and CD8 T cells from naïve mice B) Frequency of $Ki67^+$ cells in pop1-4 at week 2 and 8 p.i. C) Percentage of $Ki67^+$ cells in pop1-4 at week 2, 5, and 8 p.i. D) Intracellular staining for IFNγ and CD107a in pop1-4 at week 5 p.i. E) Percentage of $IFN\gamma^+CD107a^+$ cells from pop1-4 at week 2 and 8 p.i. F) Kinetics of the frequency $IFN\gamma^+CD107a^+$ cells from pop1-4 at week 2, 5, and 8 p.i. G) Spider plot for pop1-4 shows the frequency of $IFN\gamma^+$, $TNF\alpha^+$, and $CD107a^+$ cells from the different populations at weeks 2, 5, and 8 p.i. B, C, E, and F: Data presented as the mean for individual mice ± SEM compiled from at least 2 experiments. *$p<0.05$, **$p<0.01$, ***$p\leq0.001$, and ****$p<0.001$ (one-way ANOVA with Bonferroni post-test).

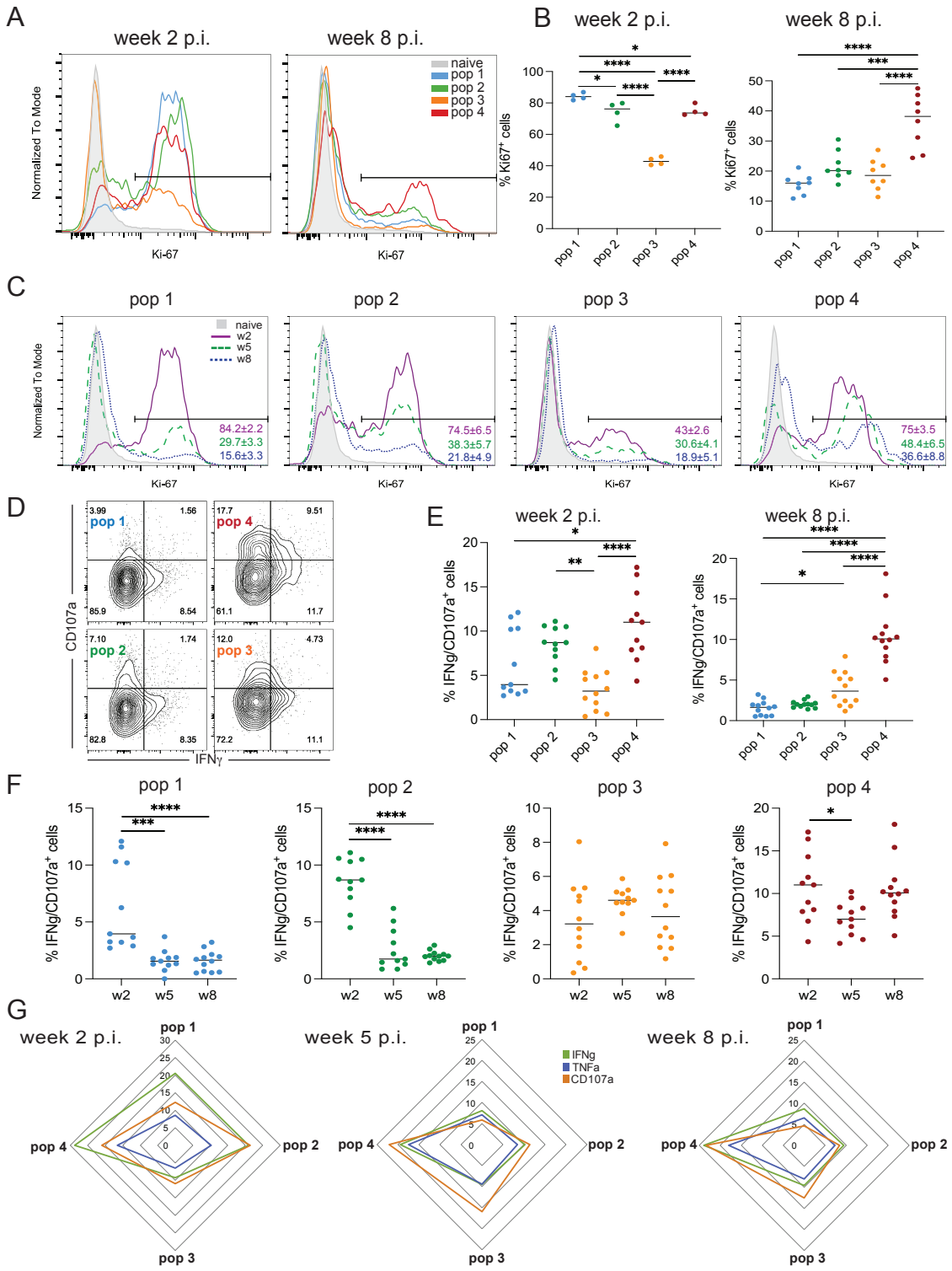
A
week 2 p.i.
week 8 p.i.
Normalized To Mode
Ki-67
naive
pop 1
pop 2
pop 3
pop 4
B
week 2 p.i.
week 8 p.i.
% Ki67+ cells
pop 1
pop 2
pop 3
pop 4
C
pop 1
pop 2
pop 3
pop 4
naive
w2
w5
w8
84.2±2.2
29.7±3.3
15.6±3.3
74.5±6.5
38.3±5.7
21.8±4.9
43±2.6
30.6±4.1
18.9±5.1
75±3.5
48.4±6.5
36.6±8.8
D
CD107a
IFNγ
3.99
1.56
85.9
8.54
17.7
9.51
61.1
11.7
7.10
1.74
82.8
8.35
12.0
4.73
72.2
11.1
E
week 2 p.i.
week 8 p.i.
% IFNg/CD107a+ cells
F
pop 1
pop 2
pop 3
pop 4
% IFNg/CD107a+ cells
w2
w5
w8
G
week 2 p.i.
week 5 p.i.
week 8 p.i.
IFNg
TNFa
CD107a